Geomechanics for Energy and the Environment 21 (2020) 100149

Contents lists available at ScienceDirect

Geomechanics for Energy and the Environment

journal homepage: www.elsevier.com/locate/gete

Analytical models for onset of sand production under isotropic and anisotropic stresses in laboratory tests

E. Papamichos *

Department of Civil Engineering, Aristotle University of Thessaloniki, GR-54124 Thessaloniki, Greece and SINTEF Industry, N-7465 Trondheim, Norway

ARTICLE INFO

Article history:
Received 4 May 2019
Received in revised form 14 August 2019
Accepted 28 August 2019
Available online 3 September 2019

Keywords:
Sand production
Anisotropic stresses
Sand onset
Hollow cylinder tests
Hole failure models

ABSTRACT

Four failure criteria, a simplified Mohr–Coulomb, a Mohr–Coulomb, a von Mises and a Drucker–Prager model are considered for borehole failure and sand onset predictions. The von Mises is a special case of the Drucker–Prager. The resulting analytical expressions are suitable for implementation in the analytical software for sand onset and sand mass analyses. The models are calibrated and validated against experimental data for hollow cylinder and hollow prism tests on Red Wildmoor sandstone. The analysis shows that a Drucker–Prager model is necessary to capture the experimentally observed effect of axial stress on hole failure. The simplified Mohr–Coulomb model shows no such effect, while the Mohr–Coulomb model shows an effect only at high values of axial stress. The Drucker–Prager model can match satisfactorily the experimental results. It requires, however, the calibration of an additional material parameter which can be done on anisotropic loading hollow prism tests. The models include also a lateral stress anisotropy parameter and a field calibration factor to allow for better approximation of available field or laboratory data.

1. Introduction

Analytical sand onset prediction models use a poroelastic solution to calculate the stresses at the borehole/perforation wall as a function of in situ stresses and pore pressure and the applied depletion and drawdown. This solution is combined with a failure model to determine hole failure and sand onset. Failure is assumed to be in shear due to the stress concentration at the hole. Failed rock is subsequently transported by the weak hydrodynamic forces of the flowing fluid leading to sand production.

The failure criterion is usually for simplicity two dimensional in the plane normal to hole axis.[1–4] Thus, it does not involve the stress parallel to the axis of the hole. A shortcoming of the two-dimensional model is that it involves only the tangential stress $\sigma_{\theta i}$ at the hole wall (the radial stress σ_{ri} is zero at the hole wall) and thus there is no effect of the axial stress σ_Z. A von Mises type model was proposed by Papamichos et al.[5] while Palmer et al.[6] proposed a Menetrey–Willam[7] model originally developed for concrete failure.

Often the failure criterion is not calibrated on uniaxial compression tests since it has been shown that such calibration underestimates the hole strength. For more accurate predictions, it is calibrated instead on hole failure data from laboratory tests on Hollow Cylinders[3,8] (HC) or Hollow Prisms (HP). The latter are primarily used when fully anisotropic stresses are applied and are prismatic cubes with a hole in one direction. Papamichos et al.[5] model was calibrated on test results from isotropically and anisotropically stressed HC and HP specimens of Red Wildmoor sandstone. Fig. 1a shows such a HP where the applied external stresses σ_{re} and σ_{Re} denote the minor and major lateral stresses, respectively, and σ_Z the axial stress. In HC specimens, isotropic lateral stresses are applied in which case $\sigma_{re} = \sigma_{Re}$, as shown in Fig. 1b. In the HC test, the applied axial stress is often equal to the applied lateral stresses. In that case the test is fully isotropic with $\sigma_Z = \sigma_{re} = \sigma_{Re}$. The hole of radius r_i is usually unsupported, in which case the internal radial stress $\sigma_{ri} = 0$ and the shear stresses $\sigma_{r\theta i} = \sigma_{z\theta i} = 0$. Fig. 2 shows a cross section normal to the hole axis and illustrates the tangential stress $\sigma_{\theta i}$ and radial stress σ_{ri} at the hole. In addition to the applied stresses, fluid is often flowed radially towards the hole by applying an external pore pressure p_e while the internal pore pressure at the hole remains ambient, i.e. $p_i = 0$.

As alternatives to two-dimensional hole failure models, this paper will employ three-dimensional models and will investigate and qualify these models on how well they capture the effect of stress anisotropy in hole failure. Representative three-dimensional models for rock and soil are the Mohr–Coulomb (MC), the von Mises (VM) and the Drucker–Prager (DP) models. The models will be calibrated on available HC/HP hole failure data for Red Wildmoor sandstone5. Red Wildmoor is a weak Triassic

* Correspondence to: Department of Civil Engineering, Aristotle University of Thessaloniki, GR-54124 Thessaloniki, Greece.
E-mail addresses: epapamic@civil.auth.gr, euripides.papamichos@sintef.no.

https://doi.org/10.1016/j.gete.2019.100149

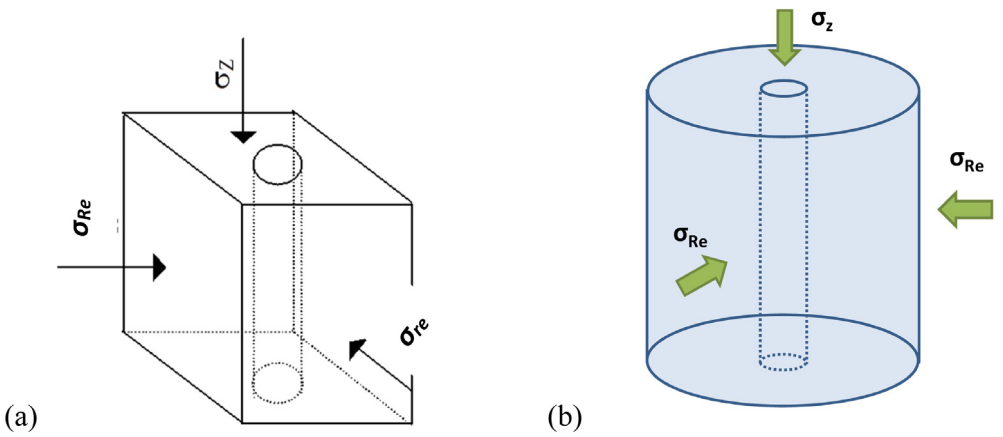

Fig. 1. Schematic of (a) a Hollow Prism (HP) specimen under anisotropic stresses σ_{re}, σ_{Re} and σ_z, and (b) a Hollow Cylinder (HC) specimen under isotropic lateral stress σ_{Re} and axial stress σ_Z.

Sherwood outcrop sandstone from Wildmoor in Bromsgrove UK. Because of its strength and petrophysical and mineralogical properties, it has been used as an analogue of weak North Sea reservoir sandstones.[9,10] It is relatively fine grained and well-sorted with a 25.8% porosity and a mean grain diameter of 0.107 mm.[11] The grains are sub-rounded, and the matrix is not well cemented. A thin coating with pore lining smectite with microcrystals of goethite and amorphous iron may be seen around the grains producing a red color. The grain contacts are relatively large due to pressure dissolution along the contact points and are cemented by the clay minerals. Red Wildmoor is water sensitive due to its high smectite content. Other models like Hoek and Brown could also be employed and calibrated on HC failure data using similar procedures.

Analytical models that can capture full three-dimensional stress anisotropy for improved sand onset and sand mass predictions from boreholes or perforations in the field are important in petroleum engineering. For such predictions the geomechanical engineers need analytical models to analyze long borehole sections (possibly of several km) using log data. Numerical analyses are possible but only on certain locations. The analytical models must therefore try to capture as much as possible of the complex behavior of the rock, the anisotropic in situ stress field and the hole geometry and inclination. In this paper, the effort has been to test and calibrate different models on how well they perform on predicting hollow cylinder and hollow prism test data and how these models are calibrated on the aforementioned tests. This is necessary because calibration in e.g. uniaxial and/or triaxial compression tests, does not account for the geometry of the problem and underestimates the predicted hole failure stresses. Rock anisotropy is currently not considered in this modeling.

The approach that is used here and in other analytical sand onset models is to use poroelasticity to calculate the stresses at the hole surface and subsequently use these stresses in a failure criterion. Since no analytical solutions exist for (hardening) plasticity models where stiffness and dilation vary with straining (something that can be successfully treated numerically), a compromise has been sought to account for plasticity. This involves the calibration of the proposed models not on failure data from uniaxial/triaxial tests but on test data from HC/HP tests which have the same geometry as boreholes and perforations in the field. This extrapolation attempts to account for the plasticity before failure. Papamichos and Furui[11] compare these analytical models with numerical predictions in field applications to see how well this assumption is valid. Material anisotropy either in the elastic parameters or in the failure criterion is not considered presently.

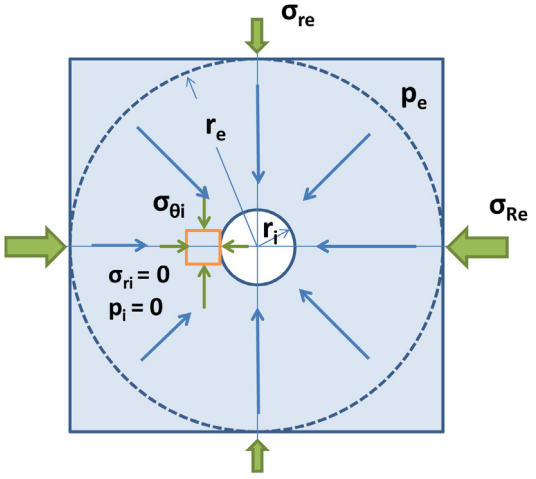

Fig. 2. Horizontal cross section (normal to the hole axis) of a HP (or HC) specimen under external stresses σ_{re}, σ_{Re} and external pore pressure p_e showing the radial $\sigma_{\theta i}$ and tangential $\sigma_{\theta i}$ stresses at the hole.

The simplified analytical approach that is employed in this analysis should not underestimate the actual complexity of sand onset and borehole stability prediction analyses which is related not only to the nonlinear behavior of the rock but also to the borehole failure mechanisms and near wellbore localization phenomena which among other lead to size effects for the failure stresses with respect to the hole size. Numerical analyses of such problems involving continua with microstructure have proven capable to simulate both qualitatively and quantitatively many of the experimental results[12–21] although challenges remain especially in the differentiation between the failure modes and post-failure simulation of sand production.

Section 2 describes the relevant stresses for the HC/HP test problem and how the stresses at the hole are derived under anisotropic stress conditions. Section 3 gives the formulation of the various models and their application and calibration on HC/HP test data on Red Wildmoor sandstone.[5] The predictions are then compared with the experimental results. Section 4 presents the conclusions. Appendix presents the necessary formulas for the poroelastic solution for the stresses and strains around the hole in a HC/HP which are necessary to derive the stresses at the hole. The poroelastic medium has elastic Young's modulus E, elastic Poisson's ratio ν and Biot's effective stress coefficient α. The elastic shear modulus is $G = E/2(1+\nu)$. The polar

coordinate system (r, θ, z) is used with σ_j, ε_j $(j = r, \theta, z)$ denoting the normal components of the stresses and strains and σ_{jk}, ε_{jk} $(j, k = r, \theta, z)$ denoting the shear components of stresses and strains, respectively. The stress and strain components at the hole are denoted with a subscript i (internal boundary) added after the last subscript of the component. Compressive stresses and strains are taken positive as usual in rock mechanics. Compressive pore fluid pressure is also positive.

2. Stresses in hollow cylinder/prism tests

The failure criteria for the hole in the HP/HC tests are based on the tangential $\sigma_{\theta i}$ and axial σ_{zi} stresses at the hole wall. The radial stress σ_{ri} and the pore pressure p_i at the hole are zero. The wall stresses can be derived from the externally applied stresses σ_{re}, σ_{Re} and σ_Z and the applied pore pressure difference $\Delta p = p_e - p_i = p_e$ between the external and internal boundary provided that a constitutive model is assumed for the rock material behavior. The simplest model is linear poroelasticity in which case the stresses at the hole wall can be obtained by applying Appendix Eqs. (50), (61) and (62) in the particular HP/HC problem with zero radial stress and pore pressure at the hole to give

$$\begin{aligned} &\sigma_{ri} = p_i = 0 \\ &\sigma_{\theta i} = \sigma_{Re} + \sigma_{re} - 2(\sigma_{Re} - \sigma_{re})\cos 2\theta - \eta_B \Delta p \left(2 - \frac{1}{\ln r_e/r_i}\right) \\ &\sigma_{zi} = \sigma_Z - 2\nu(\sigma_{Re} - \sigma_{re})\cos 2\theta - \eta_B \Delta p \left(2 + \frac{1-2\nu}{\ln r_e/r_i}\right) \end{aligned} \tag{1}$$

where η_B is the poroelastic constant

$$\eta_B = \frac{\alpha(1-2\nu)}{2(1-\nu)} \tag{2}$$

These equations hold under the assumption $r_e \gg r_i$ such that $1 - (r_i/r_e)^2 \simeq 1$. The term involving $1/\ln(r_i/r_e)$ has been kept because it does not tend rapidly to zero with increasing r_e/r_i. In typical HC tests, the ratio r_e/r_i takes values between 3 and 10. For such values, Fig. 3a shows that it is reasonable to assume that $1 - (r_i/r_e)^2 \simeq 1$. On the other hand, $1/\ln(r_e/r_i)$ is far from zero. Fig. 3b shows that for $\alpha = 1$, η_B takes values between 0.5 and 0 for values of Poisson's ratio ν between 0 and 0.5.

The maximum stresses in Eq. (1) are at an angle $\theta = 90°$ which is the direction of the minimum compressive principal stress σ_{re}. The angle θ is measured positive anticlockwise from the major compressive principal stress σ_{Re} axis. Thus, the maximum stresses at the hole wall become

$$\begin{aligned} &\sigma_{\theta i} = \sigma_{Re} + \sigma_{re} + 2\eta(\sigma_{Re} - \sigma_{re}) - \eta_B \Delta p \left(2 - \frac{1}{\ln r_e/r_i}\right) \\ &\sigma_{zi} = \sigma_Z + 2\nu\eta(\sigma_{Re} - \sigma_{re}) - \eta_B \Delta p \left(2 + \frac{1-2\nu}{\ln r_e/r_i}\right) \end{aligned} \tag{3}$$

In Eq. (3) a lateral anisotropy parameter η has been introduced to control the effect of lateral stress anisotropy on hole failure. As η increases the effect of lateral stress anisotropy on the magnitude of the hole stresses increases. For $\eta = 1$, the stresses in Eq. (3) reduce to those of linear poroelasticity. A similar expression was used in the failure criterion by Kessler et al..[1] The idea is that plasticity smooths out the stress concentration near the hole and thus anisotropy plays a smaller role than what poroelasticity may suggest.

Introducing the stress ratios

$$K_r = \sigma_{re}/\sigma_{Re} \qquad K_z = \sigma_Z/\sigma_{Re} \qquad K_p = \Delta p/\sigma_{Re} \tag{4}$$

Eq. (3) becomes

$$\sigma_{\theta i} = B_\theta \sigma_{Re} \qquad \sigma_{zi} = B_z \sigma_{Re} \tag{5}$$

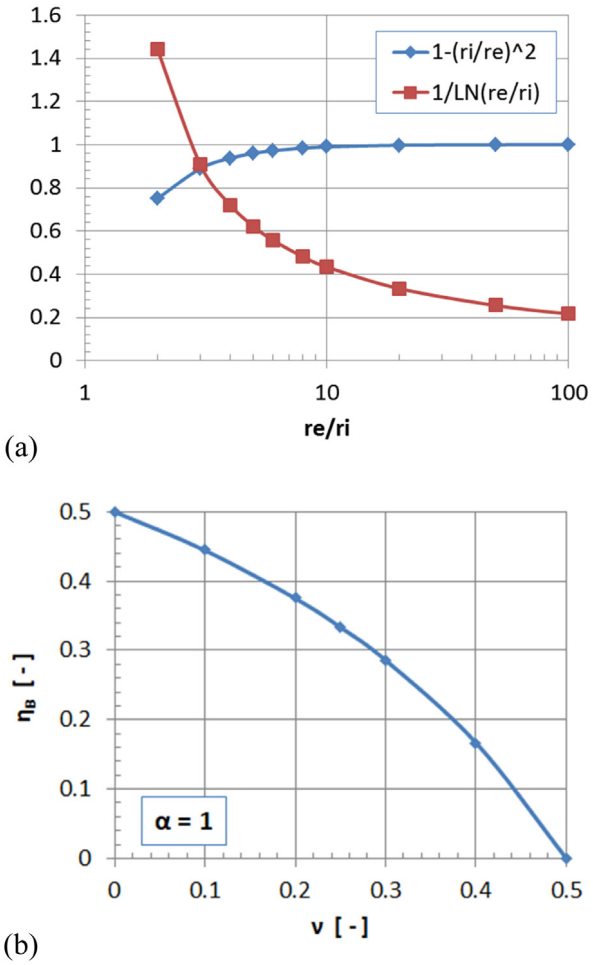

Fig. 3. (a) Functions $1 - (r_i/r_e)^2$ and $1/\ln(r_e/r_i)$vs. r_e/r_i, and (b) Parameter η_B vs. ν for $\alpha = 1$.

where

$$\begin{aligned} &B_\theta = 1 + K_r + 2\eta(1 - K_r) - \eta_B K_p \left(2 - \frac{1}{\ln r_e/r_i}\right) \\ &B_z = K_z + 2\nu\eta(1 - K_r) - \eta_B K_p \left(2 + \frac{1-2\nu}{\ln r_e/r_i}\right) \end{aligned} \tag{6}$$

In the isotropic HC/HP test with no flow, where $K_r = K_z = 1$ and $K_p = 0$, then

$$B_\theta = 2 \qquad B_z = 1 \tag{7}$$

In the following the maximum stresses at the hole are substituted in failure criteria to obtain analytical expressions for hole failure.

3. Hole failure models

Four hole failure criteria are evaluated. These criteria are based on popular rock mechanics criteria, i.e. the Mohr–Coulomb and the von Mises/Drucker–Prager criteria. Their calibration, though, is not performed through classical triaxial tests like triaxial compression tests, but through hollow cylinder/prism tests under isotropic and eventually anisotropic stress conditions.

3.1. Mohr–Coulomb model

The Mohr–Coulomb (MC) criterion can be written as

$$\sigma_1 - m\sigma_3 = k \tag{8}$$

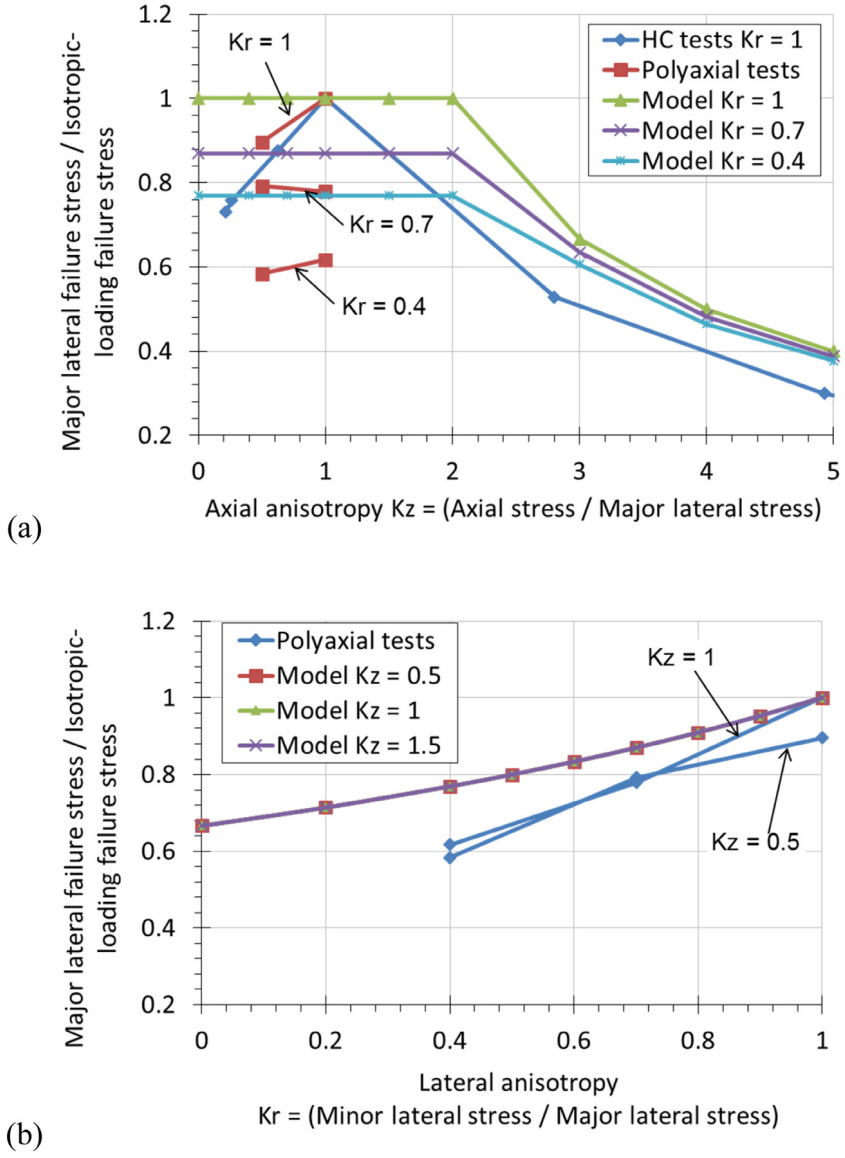

Fig. 4. Mohr–Coulomb model and isotropic and anisotropic test data on Red Wildmoor sandstone. Fit for $\nu = 0.25$ and $\eta = 1$ of the experimental data for the normalized major lateral failure stress vs. the (a) axial K_z and (b) lateral K_r anisotropy ratio.

where σ_1 and σ_3 are the major and minor principal compressive stress, respectively, and m and k two material parameters. In the HC/HP test the minor compressive principal stress $\sigma_3 = \sigma_{ri} = 0$, and therefore the MC criterion simplifies to

$$\sigma_1 = k \tag{9}$$

The same expression (9) would have been obtained if the Tresca criterion was employed instead. The Tresca criterion is a special case of the MC and is obtained by setting $m = 1$ in Eq. (8). For plane stress, as is the case for the stresses at the hole since $\sigma_{ri} = \sigma_{r\theta i} = \sigma_{zri} = 0$, the MC hole failure criterion Eq. (9) becomes

$$\sigma_{\theta i} + \sigma_{zi} + \sqrt{(\sigma_{\theta i} - \sigma_{zi})^2 + 4\sigma_{\theta zi}^2} = 2k \tag{10}$$

If calibrated on a uniaxial compression test, the material parameter k would be identified as the Uniaxial Compressive Strength (UCS). However, k is calibrated on the isotropic loading hole failure stress σ_S in HC tests. Substitution of the stresses Eq. (5) in the hole failure criterion Eq. (10) and noting that in the HC test $\sigma_{\theta zi} = 0$ yields

$$(B_\theta + B_z + |B_\theta - B_z|)\,\sigma_{Re} = 2k \tag{11}$$

where the argument in the absolute value can be positive or negative depending on whether $\sigma_{\theta i}$ or σ_{zi} is the major compressive principal stress. In the first case $B_\theta \geq B_z$ and in the second $B_z \geq B_\theta$. The material strength parameter k can be related to the isotropic-loading failure stress σ_S under no flow by applying Eq. (11) to isotropic loading and setting $\sigma_{Re} = \sigma_S$. Noting that for isotropic loading $\sigma_{\theta i} \geq \sigma_{zi}$, using Eq. (7) for B_θ and B_z and solving for k yields

$$k = 2\sigma_S \tag{12}$$

Thus, the MC hole failure criterion Eq. (11) for the HP/HC test becomes

$$\frac{1}{4}\left[B_\theta + B_z + |B_\theta - B_z|\right]\sigma_{Re} - \sigma_S = 0 \qquad \text{or} \qquad \frac{\sigma_{Re}}{\sigma_S} = \frac{4}{B_\theta + B_z + |B_\theta - B_z|} \tag{13}$$

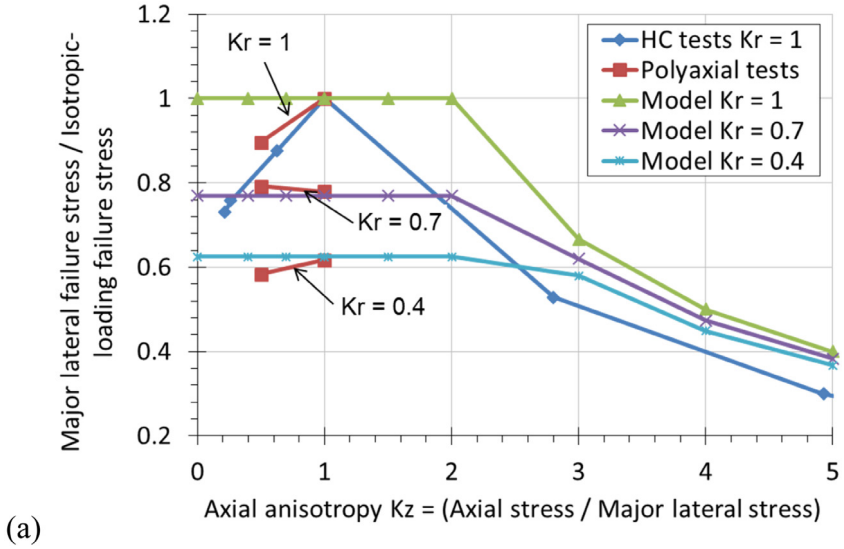

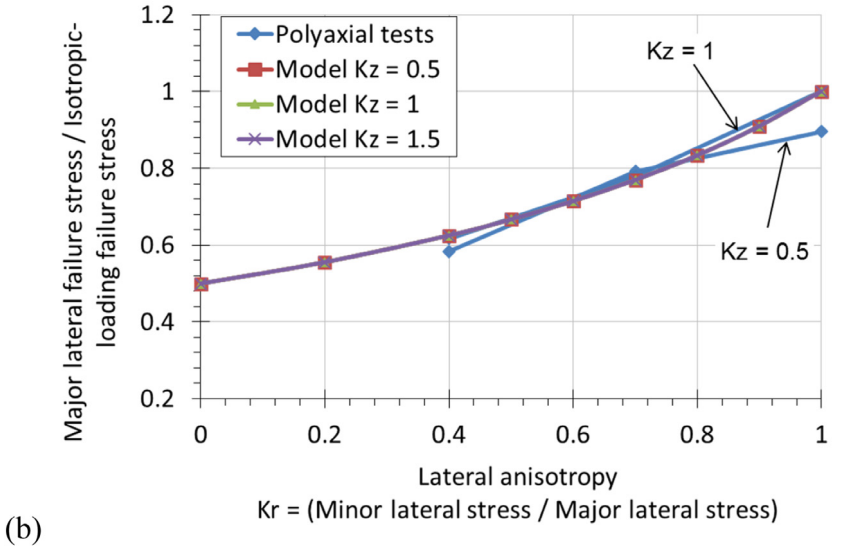

Fig. 5. Mohr–Coulomb model and isotropic and anisotropic test data on Red Wildmoor sandstone. Fit for $\nu = 0.25$ and $\eta = 1.5$ of the experimental data for the normalized major lateral failure stress vs. the (a) axial K_z and (b) lateral K_r anisotropy ratio.

Eq. (13) gives the major lateral stress for hole failure for given axial K_z and lateral K_r stress ratios and pore pressure difference ratio K_p as a function of the isotropic loading hole failure stress σ_S under no flow.

The MC failure model was calibrated on available test data from isotropically or anisotropically stressed HC/HP specimens of Red Wildmoor sandstone.[5] Fig. 4 shows the test data for stress anisotropy values $K_r = 0.4, 0.7, 1$ and $K_z = 0.5, 1, 1.5$ and the model predictions for the MC model with Poisson's ratio $\nu = 0.25$ and $\eta = 1$. Fig. 5 shows that a better fit is obtained for $\eta = 1.5$. For $K_z \leq 2$, the results are not affected by K_z. For $K_z > 2$, the hole failure stress decreases with increasing K_z.

The MC model can capture the effect of lateral stress anisotropy on hole failure where the hole failure stress decreases with increasing lateral stress anisotropy (i.e. decreasing K_r, Fig. 5b). The effect increases for $\eta > 1$ and decreases for $\eta < 1$. However, it cannot capture the effect of axial stress anisotropy for values of $K_z \leq 2$. For $K_z > 2$, the experimentally observed decrease in hole failure stress with K_z is captured.

3.1.1. Simplified Mohr–Coulomb model

A simplified MC criterion is usually used for simplicity for hole failure and sand production onset prediction.[1–4,8] The simplified MC assumes that the axial stress σ_{zi} and the shear stress $\sigma_{\theta zi}$ do not affect hole failure. Thus, only the tangential stress $\sigma_{\theta i}$ at the hole enters the failure criterion and in that case the MC hole failure criterion Eq. (10) reduces to

$$\sigma_{\theta i} = k \tag{14}$$

For the isotropic HP/HC test where $\sigma_{\theta zi} = 0$ and $\sigma_{\theta i} \geq \sigma_{zi}$, the MC and simplified MC criteria coincide and thus k is given by the same Eq. (12) as $k = 2\sigma_S$. However, in general, e.g. deviated wells, high axial stress, etc., the two criteria do not coincide. For this model, the hole failure criterion for the HP/HC test becomes

$$\frac{B_\theta}{2}\sigma_{Re} - \sigma_S = 0 \qquad \text{or} \qquad \frac{\sigma_{Re}}{\sigma_S} = \frac{2}{B_\theta} \tag{15}$$

which gives the major lateral stress for hole failure for given lateral stress ratio K_r and pore pressure difference ratio K_p as a function of the isotropic loading hole failure stress σ_S under no flow. The criterion is independent of the axial stress ratio K_z.

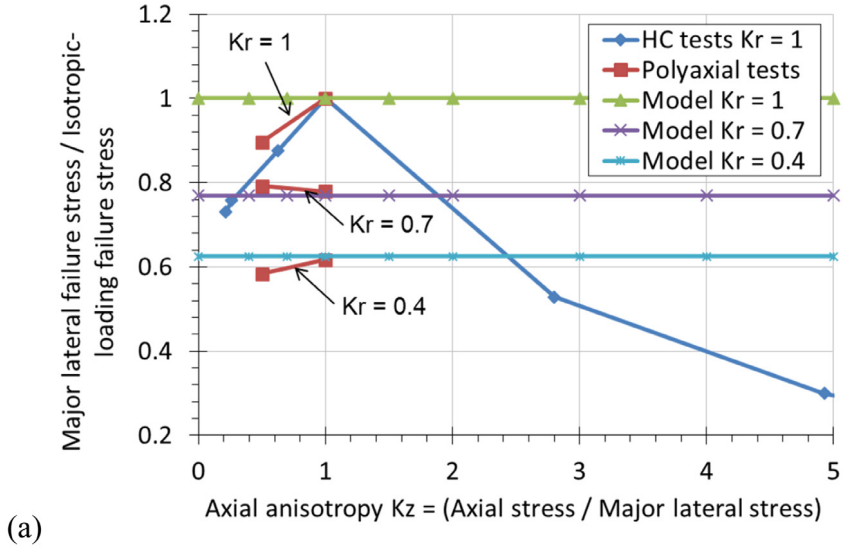

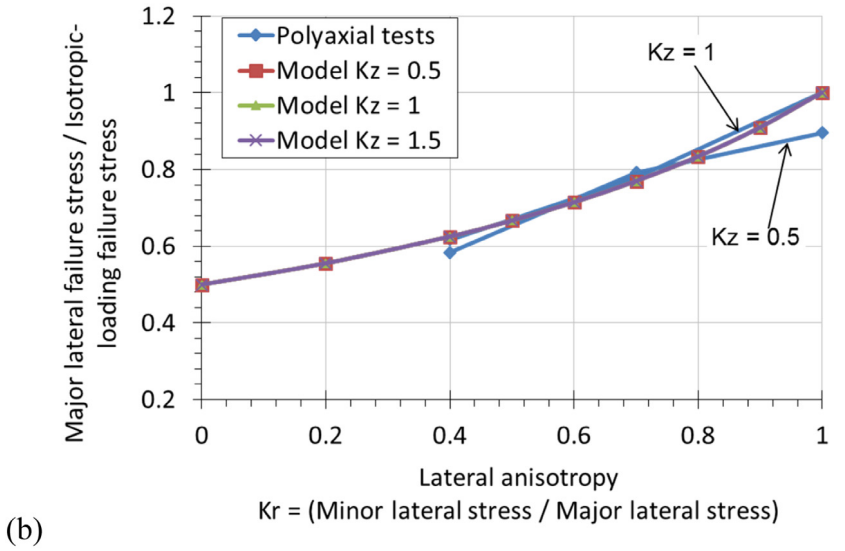

Fig. 6. Simplified Mohr–Coulomb model and isotropic and anisotropic test data on Red Wildmoor sandstone. Fit for $\eta = 1.5$ of the experimental data for the normalized major lateral failure stress vs. the (a) axial K_z and (b) lateral K_r anisotropy ratio.

Fig. 6 compares the model predictions with the test data for stress anisotropy values $K_r = 0.4, 0.7, 1$ and $K_z = 0.5, 1, 1.5$ as used in the experiments. The results are independent of the Poisson's ratio ν since σ_{zi}, which is affected by ν, does not enter the failure criterion. The parameter $\eta = 1.5$ as in Fig. 5 and to have a better fit of the data.

3.2. Von Mises model

The von Mises (VM) criterion can be written as

$$3J_2 - k^2 = 0 \tag{16}$$

where J_2 is the second deviatoric stress invariant. For plane stress, as is the case for the stresses at the hole since $\sigma_{ri} = \sigma_{r\theta i} = \sigma_{zri} = 0$, the VM criterion can be written as

$$\sigma_{\theta i}^2 + \sigma_{zi}\,(\sigma_{zi} - \sigma_{\theta i}) + 3\sigma_{\theta zi} = k^2 \tag{17}$$

If calibrated on a uniaxial compression test, the material parameter k is identified as $k =$ UCS. However, k is calibrated on the isotropic loading hole failure stress σ_S in HC tests. Substitution of the stresses Eq. (5) into the hole failure criterion Eq. (17) and noting that in the HC test $\sigma_{\theta zi} = 0$ yields

$$\sigma_{Re}^2\left[B_\theta^2 + B_z\,(B_z - B_\theta)\right] = k^2 \tag{18}$$

The material strength parameter k can be related to the isotropic loading failure stress σ_S under no flow by applying Eq. (18) and setting $\sigma_{Re} = \sigma_S$. Using Eq. (7) for B_θ and B_z and solving for k yields

$$k = \sigma_S\sqrt{3} \tag{19}$$

Thus, the HP/HC hole failure criterion Eq. (18) becomes

$$\frac{\sqrt{3}}{\sqrt{B_\theta^2 + B_z\,(B_z - B_\theta)}}\sigma_{Re} - \sigma_S = 0 \qquad \text{or} \qquad \frac{\sigma_{Re}}{\sigma_S} = \sqrt{\frac{3}{B_\theta^2 + B_z\,(B_z - B_\theta)}} \tag{20}$$

Eq. (20) gives the major lateral stress for hole failure for given axial K_z and lateral K_r stress ratios and pore pressure difference

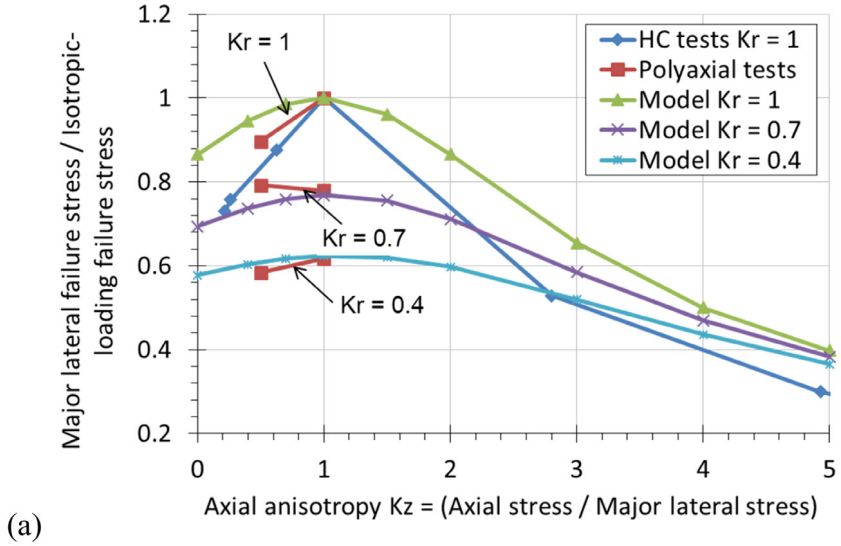

Fig. 7. Von Mises model and isotropic and anisotropic test data on Red Wildmoor sandstone. Fit for $\nu = 0.25$, $\eta = 1.5$ of the data for the normalized major lateral failure stress vs. the (a) axial K_z and (b) lateral K_r anisotropy ratio.

ratio K_p as a function of the isotropic loading hole failure stress σ_S under no flow.

Fig. 7 compares the test data with the model predictions for Poisson's ratio $\nu = 0.25$ and $\eta = 1.5$ as in the simulations with previous models. Figs. 8 and 9 show the effect of Poisson's ratio with predictions for $\nu = 0$ and 0.5.

The VM model shows an axial stress effect for all values of K_z. The maximum failure stress with respect to the axial stress anisotropy is obtained for

$$B_z = \frac{B_\theta}{2} \tag{21}$$

For the HC/HP test with no flow, this corresponds to an axial stress ratio

$$K_z = 0.5\,(1 + K_r) + \eta\,(1 - 2\nu)\,(1 - K_r) \tag{22}$$

which e.g. gives for

$$\begin{aligned} K_r = 1: &\quad \Rightarrow \quad K_z = 1 \\ K_r = 0.7: &\quad \Rightarrow \quad K_z = 0.85 + 0.3\eta\,(1 - 2\nu) \\ K_r = 0.4: &\quad \Rightarrow \quad K_z = 0.7 + 0.6\eta\,(1 - 2\nu) \end{aligned} \tag{23}$$

Thus, the highest failure stress is for isotropic loading $K_r = K_z = 1$. For $K_r \neq 1$, the highest failure stress is for K_z values close to 1 either smaller or larger depending on the Poisson's ratio and η. For $\nu = 0.25$ and $\eta = 1$, the highest failure stress is obtained for $K_z = 1$ independently of the value of K_r (cf. Fig. 9). With increasing ν the highest failure stress is obtained at lower values of K_z. On the other hand, with increasing η the highest stress is obtained at higher values of K_z. For example, for the plots in Fig. 7 to Fig. 9 for $\eta = 1.5$, Table 1 lists the K_z value at the highest failure stress for a given K_r ratio.

3.3. Drucker–Prager model

The Drucker–Prager (DP) criterion for compression positive can be written as

$$-I_1 k_1 + \sqrt{3J_2} - k = 0 \tag{24}$$

where I_1 is the first stress invariant and k_1, k are material parameters. For plane stress, as is the case for the stresses at the hole, the DP criterion can be written in terms of the principal stresses

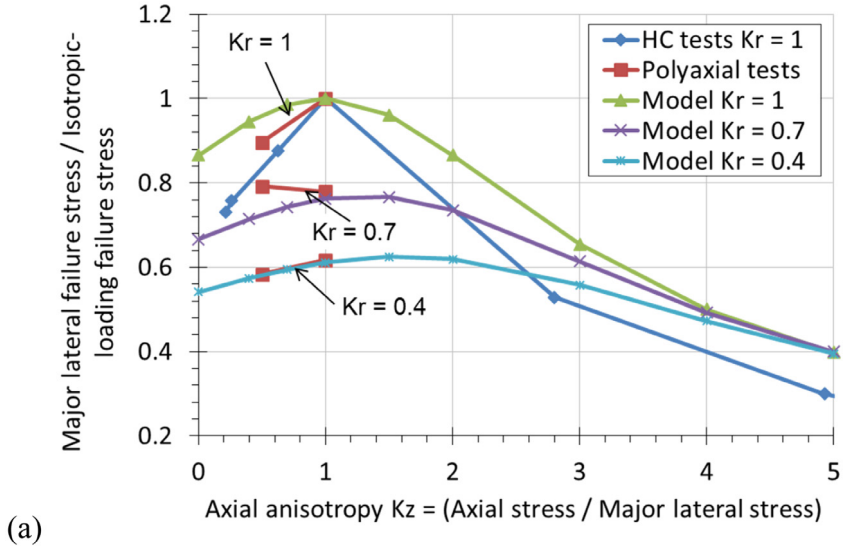

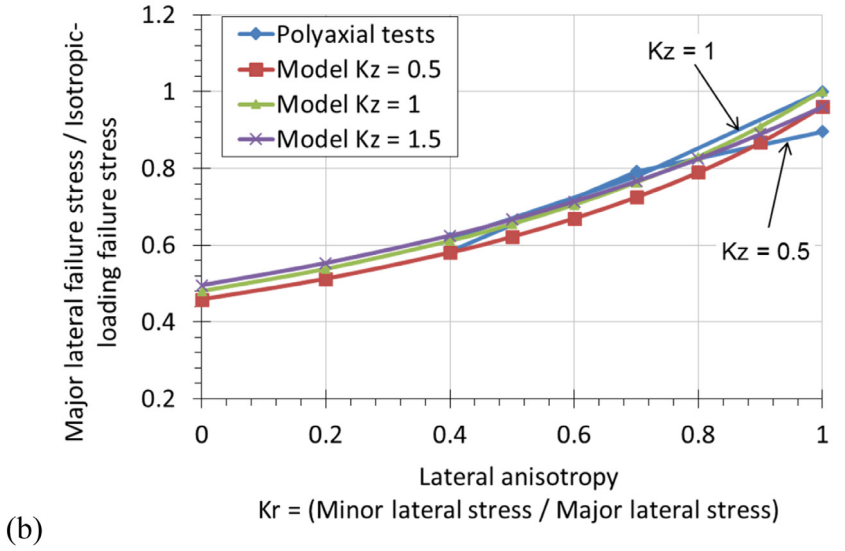

Fig. 8. Von Mises model and isotropic and anisotropic test data on Red Wildmoor sandstone. Fit for $\nu = 0$, $\eta = 1.5$ of the data for the normalized major lateral failure stress vs. the (a) axial K_z and (b) lateral K_r anisotropy ratio.

Table 1
Axial stress anisotropy ratio K_z at peak failure stress for given K_r and Poisson's ratio ν and $\eta = 1.5$.

$\eta = 1.5$		Axial stress anisotropy ratio K_z at peak failure stress		
Poisson's ratio $\nu \downarrow$	Lateral anisotropy ratio $K_r \rightarrow$	0.4	0.7	1
	0	1.6	1.3	1
	0.25	1.15	1.075	1
	0.5	0.7	0.85	1

σ_α and σ_β, as follows

$$-\left(\sigma_a + \sigma_\beta\right) k_1 + \sqrt{\sigma_a^2 - \sigma_a\sigma_\beta + \sigma_\beta^2} = k \tag{25}$$

If calibrated on uniaxial and triaxial compression tests, the material parameters k_1 and k can be expressed through the friction angle φ and the *UCS*

$$k_1 = \sin\varphi \qquad k = (1 - \sin\varphi)\, UCS \tag{26}$$

However, one of the two parameters is calibrated on the isotropic loading hole failure stress σ_S in HC tests with no flow. The other parameter can be calibrated on anisotropic loading HP test data to best fit the experimental results. Substitution of the axial σ_{zi} and tangential $\sigma_{\theta i}$ stresses at the hole in Eq. (25) leads to

$$-\left(\sigma_{zi} + \sigma_{\theta i}\right) k_1 + \sqrt{\sigma_{\theta i}^2 + \sigma_{zi}\left(\sigma_{zi} - \sigma_{\theta i}\right) + 3\sigma_{\theta zi}^2} = k \tag{27}$$

For $k_1 = 0$, the DP criterion reduces to the VM criterion in Eq. (17). Substitution of the stresses at the hole Eq. (5) in the DP criterion Eq. (27) and noting that in the HP/HC test $\sigma_{\theta zi} = 0$ yields

$$-\sigma_{Re}\left(B_\theta + B_z\right) k_1 + \sigma_{Re}\sqrt{B_\theta^2 + B_z\left(B_z - B_\theta\right)} = k \tag{28}$$

The material strength parameter k can be related to the isotropic loading failure stress σ_S under no flow by applying Eq. (28) to isotropic loading and setting $\sigma_{Re} = \sigma_S$. Using Eq. (7) for B_θ and B_z

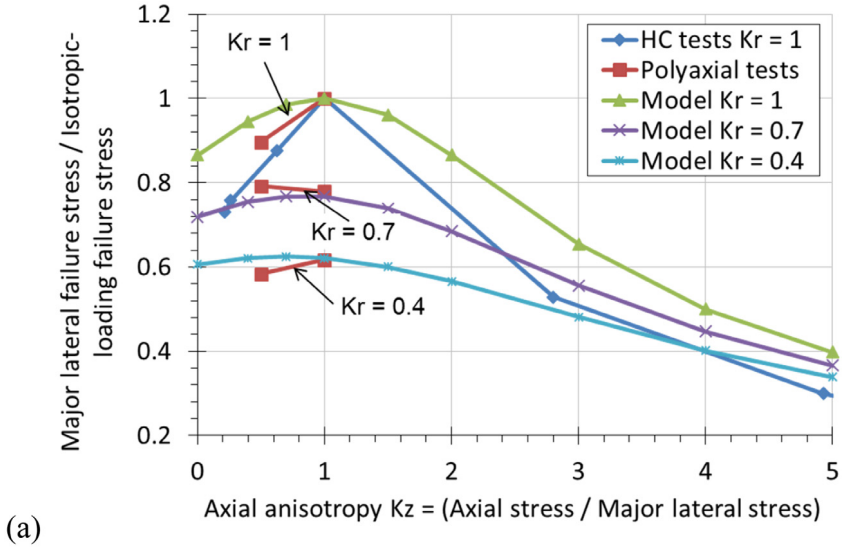

Fig. 9. Von Mises model and isotropic and anisotropic test data on Red Wildmoor sandstone. Fit for $\nu = 0.5$, $\eta = 1.5$ of the data for the normalized major lateral failure stress vs. the (a) axial K_z and (b) lateral K_r anisotropy ratio.

and solving for k yields

$$k = \left(-3k_1 + \sqrt{3}\right)\sigma_S \tag{29}$$

Thus, the hole failure criterion Eq. (28) becomes

$$\frac{-\left(B_\theta + B_z\right)k_1 + \sqrt{B_\theta^2 + B_z\left(B_z - B_\theta\right)}}{-3k_1 + \sqrt{3}}\sigma_{Re} - \sigma_S = 0$$

or (30)

$$\frac{\sigma_{Re}}{\sigma_S} = \frac{-3k_1 + \sqrt{3}}{-\left(B_\theta + B_z\right)k_1 + \sqrt{B_\theta^2 + B_z\left(B_z - B_\theta\right)}}$$

For no fluid flow and $\eta = 1$, then $B_\theta = 3 - K_r$, $B_z = K_z + 2\nu\left(1 - K_r\right)$ and the hole failure criterion Eq. (30) reduces to Eq. (31) in Box I.

Expression (31) describes a hole failure criterion independent of the lateral η anisotropy parameters. This is a simplification since η is an additional parameter introduced to better match experimental results. Fig. 10 shows the test data and the model predictions for Poisson's ratio $\nu = 0.25$, friction parameter $k_1 = 0.2$ for $\eta = 1.4$ which gives a better fit to the data.

The DP model shows an axial stress effect for all values of K_z. The highest failure stress with respect to the axial stress anisotropy K_z is obtained for

$$B_z = \frac{B_\theta}{2}\left[1 + \sqrt{\frac{3}{1/k_1^2 - 1}}\right] \tag{32}$$

For the HC/HP test with no flow, this corresponds to an axial stress ratio

$$\begin{aligned} K_z &= -2\nu\eta\left(1 - K_r\right) + \frac{B_\theta}{2}\left[1 + \sqrt{\frac{3}{1/k_1^2 - 1}}\right] = \\ &= \frac{1 + K_r}{2} + \left(1 - 2\nu\right)\eta\left(1 - K_r\right) \\ &\quad + \frac{1 + K_r + 2\nu\eta\left(1 - K_r\right)}{2}\sqrt{\frac{3}{1/k_1^2 - 1}} \end{aligned} \tag{33}$$

$$\frac{\sigma_{Re}}{\sigma_S} = \frac{-3k_1 + \sqrt{3}}{-\left[3 + 2\nu + K_z - (1+2\nu)\,K_r\right]k_1 + \sqrt{(3-K_r)^2 - \left[K_z + 2\nu\,(1-K_r)\right]\left[3 - 2\nu - K_z - (1-2\nu)\,K_r\right]}} \tag{31}$$

Box I.

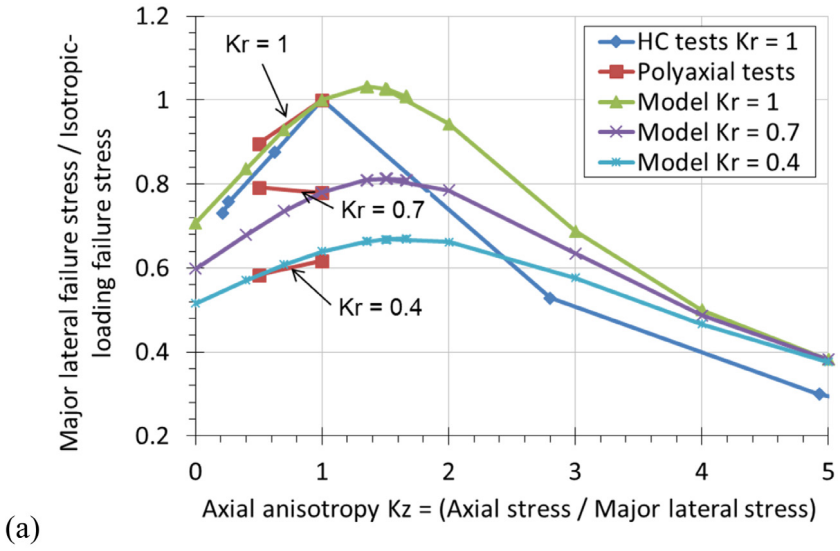

(a)

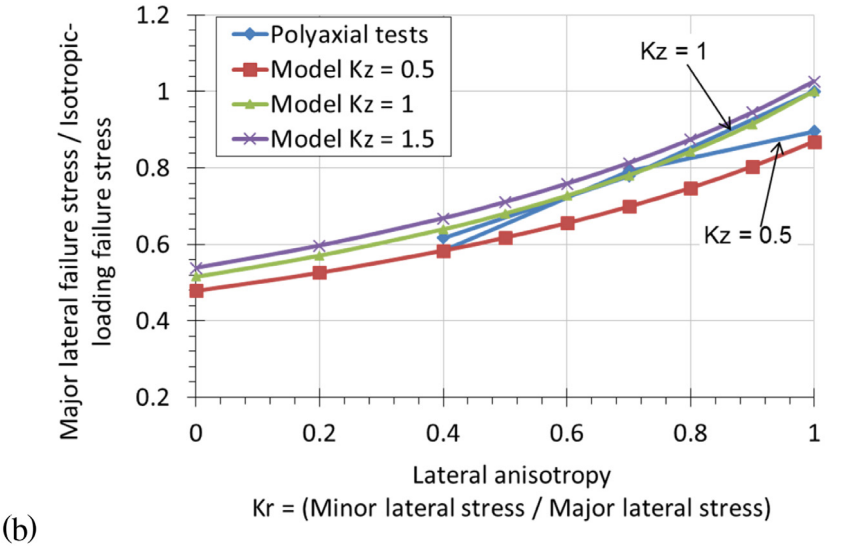

(b)

Fig. 10. Drucker–Prager model and isotropic and anisotropic test data on Red Wildmoor sandstone. Fit for $\nu = 0.25$, $\eta = 1.4$ and $k_1 = 0.2$ of the experimental data for the normalized major lateral failure stress vs. the (a) axial K_z and (b) lateral K_r anisotropy ratio.

which e.g. gives for

$$\begin{aligned}
K_r = 1: \quad &\Rightarrow \quad K_z = 1 + \sqrt{\frac{3}{1/k_1^2 - 1}} \\
K_r = 0.7: \quad &\Rightarrow \quad K_z = 0.85 + 0.3\,(1-2\nu)\,\eta \\
&\qquad + (0.85 + 0.3\eta)\sqrt{\frac{3}{1/k_1^2 - 1}} \\
K_r = 0.4: \quad &\Rightarrow \quad K_z = 0.7 + 0.6\,(1-2\nu)\,\eta \\
&\qquad + (0.7 + 0.6\eta)\sqrt{\frac{3}{1/k_1^2 - 1}}
\end{aligned} \tag{34}$$

Thus, the highest failure stress for $K_r = 1$ is at $K_z \geq 1$ and it is independent of η and ν. For $K_r \neq 1$, the highest failure stress is at K_z values usually larger than 1. With increasing ν the highest failure stress is obtained at lower values of K_z. On the other hand, with increasing η the highest stress is obtained at higher values of K_z. For example, for $\eta = 1.5$, $k_1 = 0.2$, Table 2 lists the K_z value at the highest failure stress for a given K_r ratio and Poisson's ratio ν. A comparison of the values in Table 2 for DP and Table 1 for VM shows that the effect of the friction parameter k_1 is to shift the peak towards higher K_z values.

The failure criterion Eq. (30) cannot predict failure when either the nominator or denominator are non-positive. A non-positive

Table 2
Axial stress anisotropy ratio K_z at peak failure stress for given K_r and Poisson's ratio ν and $\eta = 1.5, k_1 = 0.2$.

$\eta = 1.5, k_1 = 0.2$		Axial stress anisotropy ratio K_z at peak failure stress f		
Poisson's ratio $\nu \downarrow$	Lateral anisotropy ratio $K_r \rightarrow$	0.4	0.7	1
	0	2.166	1.760	1.354
	0.25	1.716	1.535	1.354
	0.5	1.266	1.311	1.354

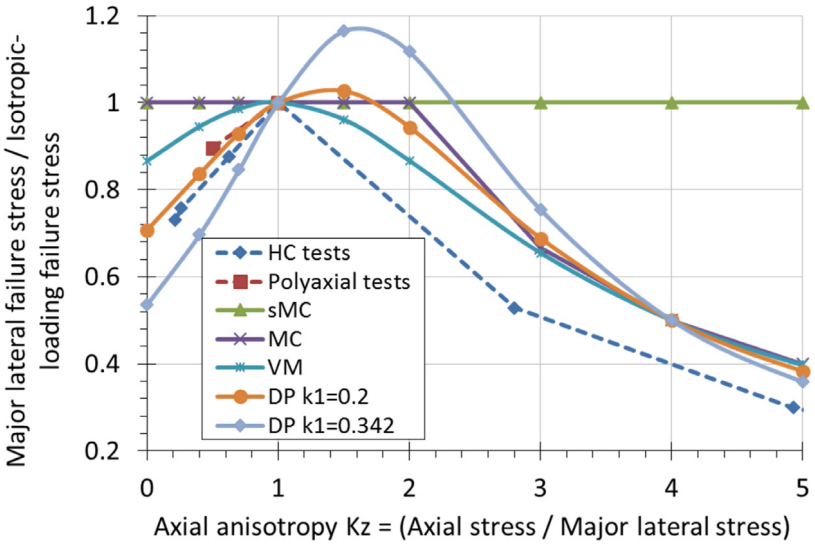

Fig. 11. Normalized major lateral stress at failure predictions by the various models and isotropic and anisotropic test data on Red Wildmoor sandstone as a function of axial stress anisotropy K_z. Comparison of the simplified Mohr–Coulomb (sMC), Mohr–Coulomb (MC), von Mises (VM), Drucker–Prager with $k_1 = 0.2$ (DP k1 = 0.2) and Drucker–Prager with $k_1 = 0.342$ (DP k1 = 0.342) models.

nominator or denominator means that hole failure is not predicted under isotropic or anisotropic loading, respectively. This yields the following condition for k_1

$$k_1 < Min\left[\frac{1}{\sqrt{3}} = 0.5774, \frac{\sqrt{B_\theta^2 + B_z\,(B_z - B_\theta)}}{B_\theta + B_z}\right] \tag{35}$$

It can be shown with simple algebra that for any B_θ or B_z

$$\frac{1}{2} \le \frac{\sqrt{B_\theta^2 + B_z\,(B_z - B_\theta)}}{B_\theta + B_z} \tag{36}$$

with the equality holding for $B_\theta = B_z$. Thus, criterion Eq. (35) can be replaced with a simple limit

$$k_1 < 0.5 \tag{37}$$

4. Conclusions

Four hole failure criteria have been introduced to model hole failure. The criteria have been calibrated on the isotropic loading HC hole failure strength σ_S under no flow. They can be expressed through an equivalent cavity stress σ_C that is compared with the hole failure strength σ_S of the formation such that

$$\sigma_C - \sigma_S \begin{cases} < 0 & \text{No failure, No sand} \\ = 0 & \text{Hole failure, Sand onset} \\ > 0 & \text{Sand production} \end{cases} \tag{38}$$

The equivalent cavity stress σ_C in the different criteria is given as Eq. (39) in Box II.

The von Mises (VM) criterion is a special case of the Drucker–Prager (DP) criterion for $k_1 = 0$. In Eq. (39) effective stresses have been used (and not total as in the previous sections) since in general the pore pressure is not zero as is the case in the HP/HC tests without flow. Strictly speaking the hole failure strength σ_S is the hole failure stress for a HC/HP test without fluid flow. However, even in HC/HP with fluid flow, the pore pressures are usually significantly smaller than the applied stresses. Therefore, σ_S may also be obtained from HC/HP tests with fluid flow when the pore pressures are low compared to the applied stresses.

The expressions for $\sigma'_{\theta i}$ and σ'_{zi} include a lateral stress anisotropy parameter $\eta \ge 0$ that increases or decreases the effect of lateral stress anisotropy on hole failure. The default value $\eta = 1$ gives the equations of linear poroelasticity. An $\eta > 1$ increases the effect and an $\eta < 1$ decreases it. An $\eta = 0$ results in isotropic loading with magnitude the average of the two lateral stresses (cf. Eq. (3)). This parameter has been introduced to better approximate HP data on hole failure on Red Wildmoor sandstone.[5] Additional tests on other sandstones may corroborate these results and confirm the general validity of the lateral anisotropy effect observed on Red Wildmoor. The calibration of the models on HP/HC test data for Poisson's ratio $\nu = 0.25$, gave the following values for the lateral anisotropy parameter η and the friction parameter k_1:

$$\begin{array}{ll} \eta = 1.5 & \text{Simplified Mohr–Coulomb} \\ \eta = 1.5 & \text{Mohr–Coulomb} \\ \eta = 1.4, k_1 = 0.2 & \text{von Mises/Drucker–Prager} \end{array} \tag{40}$$

Thus, the effect of lateral stress anisotropy on hole failure is larger than the one predicted by linear poroelasticity.

All models contain one calibration constant k which is calibrated on the hole failure stress σ_S in isotropic loading HC/HP tests. Thus, all models, including the DP model, predict the same hole failure/sand onset under isotropic conditions. The DP model contains an additional frictional parameter k_1. This parameter influences the effect of axial stress anisotropy on hole failure and can be calibrated from axial anisotropy HC/HP test results as it was done in Eq. (40).

$$
\begin{aligned}
&\sigma_C = \frac{\sigma'_{\theta i}}{2} && \text{Simplified Mohr–Coulomb}\\
&\sigma_C = \frac{1}{4}\left[\sigma'_{\theta i} + \sigma'_{zi} + \sqrt{\left(\sigma'_{\theta i} - \sigma'_{zi}\right)^2 + 4\sigma^2_{\theta zi}}\right] && \text{Mohr–Coulomb}\\
&\sigma_C = \frac{-\left(\sigma'_{zi} + \sigma'_{\theta i}\right)k_1 + \sqrt{\sigma'^2_{\theta i} + \sigma'_{zi}\left(\sigma'_{zi} - \sigma'_{\theta i}\right) + 3\sigma^2_{\theta zi}}}{-3k_1 + \sqrt{3}},\ 0 \le k_1 < 0.5 && \text{von Mises /Drucker–Prager}
\end{aligned}
\tag{39}
$$

Box II.

Fig. 11 shows a comparison of failure predictions of the models as a function of the axial stress anisotropy ratio $K_z = \sigma_Z/\sigma_{Re}$ for $K_r = \sigma_{re}/\sigma_{Re} = 1$. The figure essentially plots the second expression in Eqs. (13), (15), (20) and (30) which is the normalized with σ_S major lateral stress at failure. The figure shows that:

(i) The simplified Mohr–Coulomb model (sMC) has no dependency on K_z and thus plots as a straight horizontal line at normalized load equal to 1.
(ii) The Mohr–Coulomb model (MC) is not a function of K_z until $K_z = 2$, i.e. while $\sigma_{\theta i} \ge \sigma_{zi}$. Thus, for $K_z \le 2$ it plots as a straight horizontal line at normalized load equal to 1. For $K_z > 2$ the load decreases with increasing K_z. Thus, for $K_z \le 2$ and in the absence of shear stress $\sigma_{\theta zi}$ at the hole, the sMC and MC criteria coincide. The shear stress is zero in vertical or horizontal holes. For deviated holes, the shear stress is non-zero and the MC prediction would be lower than the sMC for all K_z values.
(iii) The von Mises (VM) model predicts a normalized failure load less than 1 for either $K_z > 1$ or $K_z < 1$.
(iv) The Drucker–Prager (DP) model predicts a normalized failure load less than 1 for $K_z < 1$. For $K_z > 1$ it initially predicts a failure load more than 1 but as the K_z anisotropy increases, a load less than 1 is predicted. The peak of the failure stress moves from $K_z = 1$ for $k_1 = 0$ (VM model) to higher K_z values with increasing k_1. Similarly, the effect of axial stress anisotropy is amplified with increasing k_1. Thus, in a field environment, vertical holes (i.e. $K_z > 1$) will show higher strength under the DP model while horizontal holes (i.e. $K_z < 1$) will show lower strength.

As a conclusion, the results in Fig. 11 show that the sMC model is the least conservative of all models giving the higher hole failure stress, except for the DP model which may give, depending on k_1, a higher failure stress for some values of $K_z > 1$. Note that the MC, VM and DP models include also the shear stress $\sigma_{\theta zi}$ which for deviated holes further reduces the hole failure stress predictions. In the cases in Fig. 11, the shear stress $\sigma_{\theta zi} = 0$. The second least conservative is the MC model and then the VM model. The DP model shows the largest effect of K_z on failure stress, being the most conservative for $K_z < 1$, then the least conservative for $K_z > 1$ and finally again most conservative at higher $K_z \gg 1$. This effect is amplified with increasing the k_1 value.

Acknowledgment

This work has been supported by the research project "Increasing profitability of sand producing fields" funded by the PETROMAKS 2 program of the Research Council of Norway and Aker BP, Anadarko, DEA Norway and Hess (Project number 268159).

Appendix. Poro-elastic solutions for hollow cylinders

A.1. Isotropic lateral loading

The considered problem is a Hollow Cylinder (HC) of internal radius r_i and external radius r_e under isotropic external stress σ_{re}, external pore pressure p_e, internal stress σ_{ri} and internal pore pressure p_i. In the axis of the hole, a constant along r axial strain ε_z is applied (Fig. 12). Plane strain is a special case of this loading where $\varepsilon_z = 0$.

The pore pressure for steady-state flow and constant permeability is given as

$$
p = p_i + (p_e - p_i)\frac{\ln r/r_i}{\ln r_e/r_i} = p_e - (p_e - p_i)\frac{\ln r/r_e}{\ln r_i/r_e} \tag{41}
$$

The radial σ_r, tangential σ_θ and axial σ_z stresses are given as:

$$
\begin{aligned}
\sigma_r &= \sigma_{ri} + [\sigma_{re} - \sigma_{ri} - \eta_B(p_e - p_i)]\frac{1 - r_i^2/r^2}{1 - r_i^2/r_e^2}\\
&\quad + \eta_B(p_e - p_i)\frac{\ln r_i/r}{\ln r_i/r_e} =\\
&= \sigma_{re} - [\sigma_{re} - \sigma_{ri} - \eta_B(p_e - p_i)]\frac{r_i^2/r^2 - r_i^2/r_e^2}{1 - r_i^2/r_e^2}\\
&\quad - \eta_B(p_e - p_i)\frac{\ln r/r_e}{\ln r_i/r_e}\\
\sigma_\theta &= \sigma_{ri} + [\sigma_{re} - \sigma_{ri} - \eta_B(p_e - p_i)]\frac{1 + r_i^2/r^2}{1 - r_i^2/r_e^2}\\
&\quad - \eta_B(p_e - p_i)\frac{1 - \ln r_i/r}{\ln r_i/r_e} =\\
&= \sigma_{re} + [\sigma_{re} - \sigma_{ri} - \eta_B(p_e - p_i)]\frac{r_i^2/r^2 + r_i^2/r_e^2}{1 - r_i^2/r_e^2}\\
&\quad - \eta_B(p_e - p_i)\frac{1 + \ln r/r_e}{\ln r_i/r_e}\\
\sigma_z &= \nu(\sigma_r + \sigma_\theta) + \alpha(1 - 2\nu)p + E\varepsilon_z =\\
&= 2\nu\sigma_{ri} + \alpha(1 - 2\nu)p_i + [\sigma_{re} - \sigma_{ri} - \eta_B(p_e - p_i)]\frac{2\nu}{1 - r_i^2/r_e^2}\\
&\quad - \eta_B(p_e - p_i)\frac{\nu - 2\ln r_i/r}{\ln r_i/r_e} + E\varepsilon_z =\\
&= 2\nu\sigma_{re} + \alpha(1 - 2\nu)p_e + [\sigma_{re} - \sigma_{ri} - \eta_B(p_e - p_i)]\frac{2\nu r_i^2/r_e^2}{1 - r_i^2/r_e^2}\\
&\quad - \eta_B(p_e - p_i)\frac{\nu + 2\ln r/r_e}{\ln r_i/r_e} + E\varepsilon_z
\end{aligned}
\tag{42}
$$

The corresponding effective stresses σ'_r, σ'_θ and σ'_z are

$$
\begin{aligned}
\sigma'_r &= \sigma_r - \alpha p\\
\sigma'_\theta &= \sigma_\theta - \alpha p\\
\sigma'_z &= \sigma_z - \alpha p = \nu\left(\sigma'_r + \sigma'_\theta\right) + E\varepsilon_z
\end{aligned}
\tag{43}
$$

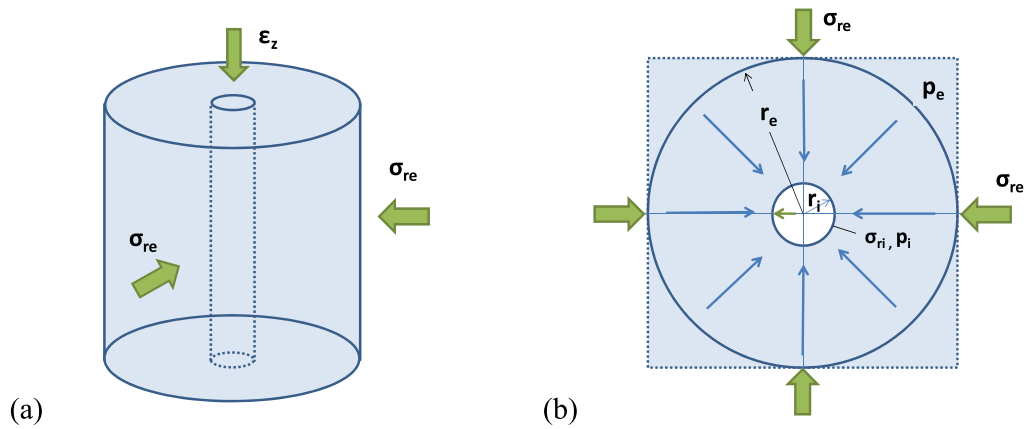

Fig. 12. Schematic of HC loading with constant along r axial strain, and (b) Loading in a cross section normal to the hole axis.

For a uniform along r axial strain ε_z, the axial stress σ_z is not constant along r. This can be seen from Eq. (42) and results from the logarithmic pore pressure term that is a function of r. Under no flow, σ_z becomes independent of r. The average axial stress $\overline{\sigma}_z$ can be calculated by integrating σ_z in Eq. (42) on a cross section normal to the hole axis

$$\begin{aligned}\overline{\sigma}_z &= \frac{2\pi\int_{r_i}^{r_e}\sigma_z r dr}{\pi\left(r_e^2-r_i^2\right)} = 2\nu\sigma_{ri} + \alpha\left(1-2\nu\right)p_i + \\ &+ \left[2\nu\left(\sigma_{re}-\sigma_{ri}\right)+\alpha\left(1-2\nu\right)\left(p_e-p_i\right)\right]\frac{1}{1-r_i^2/r_e^2} \\ &- \eta_B\left(p_e-p_i\right)\frac{1-\nu}{\ln r_i/r_e} + E\varepsilon_z\end{aligned} \tag{44}$$

Eq. (44) is useful in the analysis of the typical HC test where an isotropic confining stress is applied all around the specimen. In the axial direction, the loading takes place through a steel (assumed rigid) platen such that in reality a uniform axial strain is applied which can be calculated from Eq. (44) as

$$\begin{aligned}E\varepsilon_z &= \overline{\sigma}_z - 2\nu\sigma_{ri} - \alpha\left(1-2\nu\right)p_i \\ &- \left[2\nu\left(\sigma_{re}-\sigma_{ri}\right)+\alpha\left(1-2\nu\right)\left(p_e-p_i\right)\right]\frac{1}{1-r_i^2/r_e^2} + \\ &+ \eta_B\left(p_e-p_i\right)\frac{1-\nu}{\ln r_i/r_e}\end{aligned} \tag{45}$$

To satisfy force equilibrium, the uniform axial strain is such that it produces an average axial stress that is equal to the applied axial stress σ_Z in the upper and lower loading platens. Often and depending on the HC setup, the axial stress is applied in a platen without a hole. This is also the case for the SINTEF HC setup. In this case, the axial stress on the specimen must be corrected for the hole cross-section. Thus, the average axial stress is related to the applied axial stress as

$$\overline{\sigma}_z = \begin{cases} \sigma_Z & \text{platen with hole} \\ \dfrac{\sigma_Z}{1-r_i^2/r_e^2} & \text{platen without hole} \end{cases} \tag{46}$$

Eqs. (45) and (46) can be used to express the poroelastic stress and strain solutions for the HC test as a function of σ_Z.

A.1.1. Large external diameter

For $r_e \gg r_i$ the solution simplifies since the term $1-r_i^2/r_e^2 \cong 1$ and Eq. (42) reduces to

$$\begin{aligned}\sigma_r &= \sigma_{ri} + \left[\sigma_{re}-\sigma_{ri}-\eta_B\left(p_e-p_i\right)\right]\left(1-\frac{r_i^2}{r^2}\right) \\ &+ \eta_B\left(p_e-p_i\right)\frac{\ln r_i/r}{\ln r_i/r_e} = \\ &= \sigma_{re} - \left[\sigma_{re}-\sigma_{ri}-\eta_B\left(p_e-p_i\right)\right]\frac{r_i^2}{r^2} - \eta_B\left(p_e-p_i\right)\frac{\ln r/r_e}{\ln r_i/r_e} \\ \sigma_\theta &= \sigma_{ri} + \left[\sigma_{re}-\sigma_{ri}-\eta_B\left(p_e-p_i\right)\right]\left(1+\frac{r_i^2}{r^2}\right) \\ &- \eta_B\left(p_e-p_i\right)\frac{1-\ln r_i/r}{\ln r_i/r_e} = \\ &= \sigma_{re} + \left[\sigma_{re}-\sigma_{ri}-\eta_B\left(p_e-p_i\right)\right]\frac{r_i^2}{r^2} - \eta_B\left(p_e-p_i\right)\frac{1+\ln r/r_e}{\ln r_i/r_e}\end{aligned} \tag{47}$$

$$\begin{aligned}\sigma_z &= \nu\left(\sigma_r+\sigma_\theta\right) + \alpha\left(1-2\nu\right)p + E\varepsilon_z = \\ &= 2\nu\sigma_{re} + \alpha\left(1-2\nu\right)p_i - \eta_B\left(p_e-p_i\right)\left(2\nu+\frac{\nu-2\ln r_i/r}{\ln r_i/r_e}\right) \\ &+ E\varepsilon_z = \\ &= 2\nu\sigma_{re} + \alpha\left(1-2\nu\right)p_e - \eta_B\left(p_e-p_i\right)\frac{\nu+2\ln r/r_e}{\ln r_i/r_e} + E\varepsilon_z\end{aligned}$$

The effective stresses σ_r', σ_θ' and σ_z' are given by Eq. (43), the average axial stress $\overline{\sigma}_z$ in Eq. (44) becomes

$$\overline{\sigma}_z = 2\nu\sigma_{re} + \alpha\left(1-2\nu\right)p_e - \eta_B\left(p_e-p_i\right)\frac{1-\nu}{\ln r_i/r_e} + E\varepsilon_z \tag{48}$$

and the uniform axial strain in Eq. (45) becomes

$$E\varepsilon_z = \overline{\sigma}_z - 2\nu\sigma_{re} - \alpha\left(1-2\nu\right)p_e + \eta_B\left(p_e-p_i\right)\frac{1-\nu}{\ln r_i/r_e} \tag{49}$$

At the HC wall, i.e. for $r = r_i$, the stresses in Eq. (47) reduce to

$$\begin{aligned}\sigma_r &= \sigma_{ri} \\ \sigma_\theta &= 2\sigma_{re} - \sigma_{ri} - \eta_B\left(p_e-p_i\right)\left(2+\frac{1}{\ln r_i/r_e}\right) \\ \sigma_z &= 2\nu\sigma_{re} + \alpha\left(1-2\nu\right)p_e - \eta_B\left(p_e-p_i\right)\left(2+\frac{\nu}{\ln r_i/r_e}\right) + E\varepsilon_z\end{aligned} \tag{50}$$

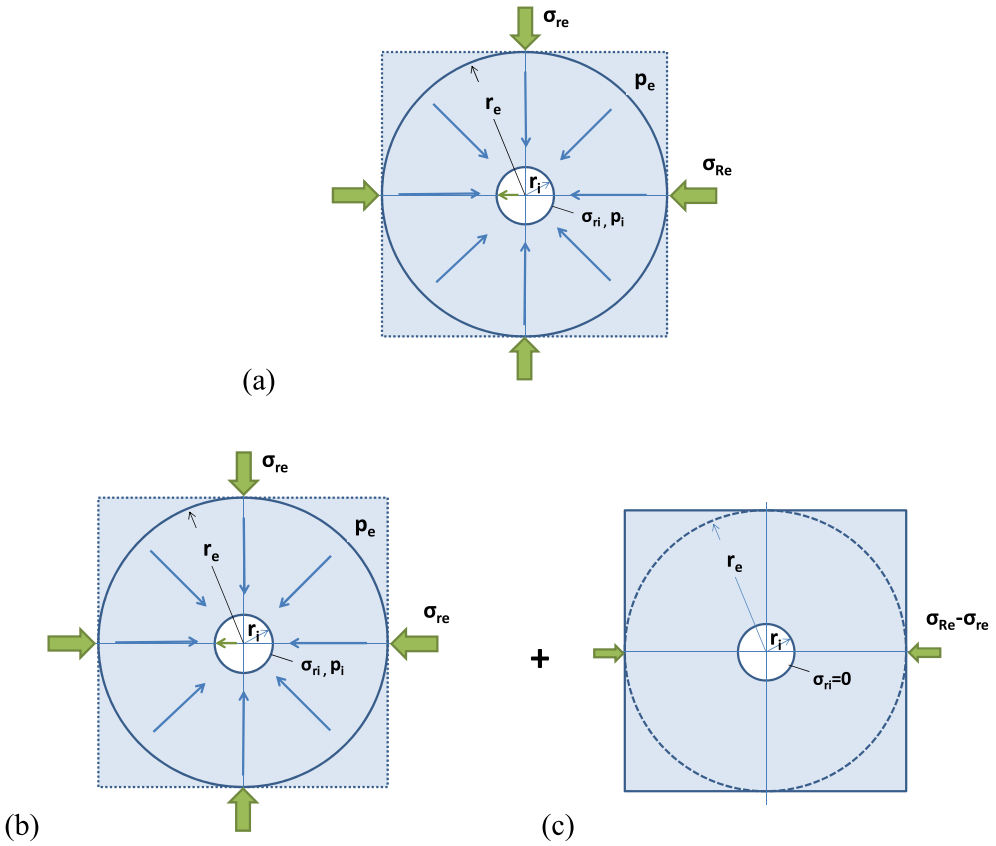

Fig. 13. Analysis of (a) anisotropic loading of a HC into (b) an isotropic loading and (c) a uniaxial loading in the direction of the major lateral stress.

A.2. Anisotropic lateral loading

The case of anisotropic lateral loading shown in Fig. 13a can be viewed as the superposition of an isotropic lateral loading (Fig. 13b) and an anisotropic loading in the direction of the major lateral stress under plane strain $\varepsilon_z = 0$ in the axial direction (Fig. 13c). The solution of the isotropic poroelastic problem is given in Appendix A.1. For the anisotropic loading, the following normal σ_r and shear $\sigma_{r\theta}$ loading is considered at radius $r = r_e$

$$\left.\begin{aligned} &\sigma_r = (\sigma_{Re} - \sigma_{re})\cos 2\theta = \frac{\sigma_{Re} - \sigma_{re}}{2} + \frac{\sigma_{Re} - \sigma_{re}}{2}\cos 2\theta \\ &\sigma_{r\theta} = -\frac{\sigma_{Re} - \sigma_{re}}{2}\sin 2\theta \\ &\text{at } r = r_e \end{aligned}\right\} \tag{51}$$

For $r_e \gg r_i$, these stresses are effectively the same as in an infinite medium without a hole under the far field stress $\sigma_{Re}-\sigma_{re}$ and thus correspond to the loading in the anisotropic problem in Fig. 13c. The solution for the radial σ_r, tangential σ_θ and shear $\sigma_{r\theta}$ stresses is given as[22, (pg. 90–92)]

$$\begin{aligned} \sigma_r &= \frac{\sigma_{Re} - \sigma_{re}}{2}\cdot\frac{1 - r_i^2/r^2}{1 - r_i^2/r_e^2} \\ &\quad + \frac{\sigma_{Re} - \sigma_{re}}{2}\left(A + 3C\frac{r_i^4}{r^4} - 2D\frac{r_i^2}{r^2}\right)\frac{\cos 2\theta}{1 - r_i^2/r_e^2} \end{aligned}$$

$$\begin{aligned} \sigma_\theta &= \frac{\sigma_{Re} - \sigma_{re}}{2}\cdot\frac{1 + r_i^2/r^2}{1 - r_i^2/r_e^2} \\ &\quad - \frac{\sigma_{Re} - \sigma_{re}}{2}\left(A - 6B\frac{r^2}{r_i^2} + 3C\frac{r_i^4}{r^4}\right)\frac{\cos 2\theta}{1 - r_i^2/r_e^2} \\ \sigma_{r\theta} &= -\frac{\sigma_{Re} - \sigma_{re}}{2}\left(A - 3B\frac{r^2}{r_i^2} - 3C\frac{r_i^4}{r^4} + D\frac{r_i^2}{r^2}\right)\frac{\sin 2\theta}{1 - r_i^2/r_e^2} \end{aligned} \tag{52}$$

where the integration constants are determined from the boundary conditions Eq. (51) at the external boundary and from the boundary condition that the hole edge is free of external forces, with solution

$$\begin{aligned} A &= \frac{1 + r_i^2/r_e^2 + 4r_i^4/r_e^4}{\left(1 - r_i^2/r_e^2\right)^2}, \qquad B = \frac{2r_i^4/r_e^4}{\left(1 - r_i^2/r_e^2\right)^2} \\ C &= \frac{1 + r_i^2/r_e^2}{\left(1 - r_i^2/r_e^2\right)^2}, \qquad D = \frac{2\left(1 + r_i^2/r_e^2 + r_i^4/r_e^4\right)}{\left(1 - r_i^2/r_e^2\right)^2} \end{aligned} \tag{53}$$

Using the equations of plane strain elasticity, the axial stress σ_z can be calculated as

$$\sigma_z = \nu\left(\sigma_r + \sigma_\theta\right) = \nu\frac{\sigma_{Re} - \sigma_{re}}{1 - r_i^2/r_e^2}\left[1 + \left(3B\frac{r^2}{r_i^2} - D\frac{r_i^2}{r^2}\right)\cos 2\theta\right] \tag{54}$$

In this loading, the effective stresses are identical to the total stresses since the pore pressure is zero. The average axial stress $\overline{\sigma}_z$ can be calculated by integrating σ_z in Eq. (54) on a cross

section normal to the hole axis

$$\overline{\sigma}_z = \frac{\int_0^{2\pi}\int_{r_i}^{r_e}\sigma_z r dr d\theta}{\pi\left(r_e^2 - r_i^2\right)} = \nu\frac{\sigma_{Re}-\sigma_{re}}{1-r_i^2/r_e^2}\cdot\frac{2\pi\int_{r_i}^{r_e} r dr}{\pi\left(r_e^2-r_i^2\right)} = \nu\frac{\sigma_{Re}-\sigma_{re}}{1-r_i^2/r_e^2} \tag{55}$$

The complete poroelastic solution for anisotropic loading can be obtained by summing the solutions for the isotropic loading Eqs. (42) and (43) with the corresponding solutions for the anisotropic loading Eqs. (52), (53) and (54). Similarly, the complete solution for the average axial stress is the sum of Eqs. (44) and (55). The uniform axial strain in Eq. (49) becomes then

$$\begin{aligned} E\varepsilon_z = {} & \overline{\sigma}_z - 2\nu\sigma_{ri} - \alpha(1-2\nu)p_i \\ & - \left[\nu\left(\sigma_{Re}+\sigma_{re}-2\sigma_{ri}\right)+\alpha(1-2\nu)\left(p_e-p_i\right)\right]\frac{1}{1-r_i^2/r_e^2} + \\ & + \eta_B\left(p_e-p_i\right)\frac{1-\nu}{\ln r_i/r_e} \end{aligned} \tag{56}$$

A.2.1. Large external diameter

For $r_e \gg r_i$, the solution simplifies since the integrations constants in Eq. (52) reduce to

$$A = 1, \qquad B = 0, \qquad C = 1, \qquad D = 2 \tag{57}$$

The anisotropic solution in this case is known as the Kirsch solution and the stresses are

$$\begin{aligned} \sigma_r &= \frac{\sigma_{Re}-\sigma_{re}}{2}\left(1-\frac{r_i^2}{r^2}\right)+\frac{\sigma_{Re}-\sigma_{re}}{2}\left(1+\frac{3r_i^4}{r^4}-\frac{4r_i^2}{r^2}\right)\cos 2\theta \\ \sigma_\theta &= \frac{\sigma_{Re}-\sigma_{re}}{2}\left(1+\frac{r_i^2}{r^2}\right)-\frac{\sigma_{Re}-\sigma_{re}}{2}\left(1+\frac{3r_i^4}{r^4}\right)\cos 2\theta \\ \sigma_{r\theta} &= -\frac{\sigma_{Re}-\sigma_{re}}{2}\left(1-\frac{3r_i^4}{r^4}+\frac{2r_i^2}{r^2}\right)\sin 2\theta \end{aligned} \tag{58}$$

The axial stress σ_z results from Eqs. (54) and (58) as

$$\sigma_z = \nu\left(\sigma_{Re}-\sigma_{re}\right)\left(1-\frac{2r_i^2}{r^2}\cos 2\theta\right) \tag{59}$$

In this loading, the effective stresses are identical to the total stresses since the pore pressure is zero. The average axial stress $\overline{\sigma}_z$ reduces to

$$\overline{\sigma}_z = \nu\left(\sigma_{Re}-\sigma_{re}\right) \tag{60}$$

The complete poroelastic solution for anisotropic loading in this case can be obtained by summing the solutions for the isotropic loading Eqs. (47) with the corresponding solutions for the anisotropic loading Eqs. (58) and (59). Similarly, the complete solution for the average axial stress is the sum of Eqs. (48) and (60). The uniform axial strain in Eq. (49) becomes then

$$E\varepsilon_z = \overline{\sigma}_z - \nu\left(\sigma_{Re}+\sigma_{re}\right) - \alpha(1-2\nu)p_e + \eta_B\left(p_e-p_i\right)\frac{1-\nu}{\ln r_i/r_e} \tag{61}$$

At the HC wall, i.e. for $r = r_i$, the stresses in Eq. (58) simplify to

$$\begin{aligned} \sigma_{ri} &= 0 \\ \sigma_{\theta i} &= \left(\sigma_{Re}-\sigma_{re}\right)\left(1-2\cos 2\theta\right) \\ \sigma_{zi} &= \nu\left(\sigma_{Re}-\sigma_{re}\right)\left(1-2\cos 2\theta\right) \\ \sigma_{r\theta i} &= 0 \end{aligned} \tag{62}$$

References

1. Kessler N, Wang Y, Santarelli F. A simplified pseudo 3D model to evaluate sand production risk in deviated cased holes. In: *SPE 26541, 68th Annual Technical Conf. and Exhibition of the SPE*. Houston: 1993.
2. van den Hoek PJ, Hertogh GMM, Kooijman AP, Bree Ph de, Kenter CJ, Papamichos E. A new concept of sand production prediction: Theory and laboratory experiments. SPE 65756, *SPE Drill Complet*. 2000;15(4):261–273.
3. Willson SM, Moschovidis ZA, Cameron JR, Palmer ID. New model for predicting the rate of sand production. In: *SPE/ISRM 78168, SPE/ISRM Rock mechanics Conference*, Irving, T.X. USA: 2002.
4. Fjær E, Holt RM, Horsrud P, Raaen AM, Risnes R. Petroleum related rock mechanics, In: Developments in Petroleum Science, 2nd ed., vol. 53, Elsevier; 2008.
5. Papamichos E, Tronvoll J, Skjærstein A, Unander TE. Hole stability of Red Wildmoor sandstone under anisotropic stresses and sand production criterion. *J Petrol Sci Eng*. 2010;72:78–92. http://dx.doi.org/10.1016/j.petrol.2010.03.006.
6. Palmer ID, Higgs N, Moschovidis Z, Cameron J. How 3D Stresses can change the standard Thick-Walled Cylinder approach to sand prediction. In: *ARMA/USRMS 05-792. 40th US Symposium on Rock Mechanics: Rock Mechanics for Energy, Mineral and Infrastructure Development in the Northern Regions*, Anchorage, AL, USA: 2005.
7. Ph Menetrey, Willam, KJ. Menetrey ph willam k.j a triaxial failure criterion for concrete and its generalization. *ACI Struct J*. 1995;92(3):311–318.
8. Veeken CAM, Davies DR, Kenter CJ, Kooijman AP. Sand production prediction review: developing an integrated approach. In: *SPE22792, 66th SPE Annual Technical Conference and Exhibition*, Dallas, T.X. USA: 1991.
9. Papamichos E, Tronvoll J, Vardoulakis I, Labuz JF, Skjærstein A, Unander TE, Sulem J. Constitutive testing of red wildmoor sandstone. *Mech Cohesive-Frict Mater*. 2000;5(1):1–40.
10. Sulem J, Vardoulakis I, Papamichos E, Oulahna A, Tronvoll J. Elasto-plastic modelling of Red Wildmoor sandstone. *Mech Cohesive-Frict Mater*. 1999;4(3):215–245.
11. Papamichos E, Furui K. Analytical models for sand onset under field conditions. *J Petrol Sci Eng*. 2019;172:171–189. http://dx.doi.org/10.1016/j.petrol.2018.09.009.
12. Papanastasiou P, Vardoulakis I. Numerical treatment of progressive localization in relation to borehole stability. *Int J Numer Anal Methods Geomech*. 1992;16:389–424.
13. Zervos A, Papanastasiou P, Vardoulakis I. Modelling localisation and scale effect in thick-walled cylinders with gradient elastoplasticity. *Int J Solids Struct*. 2001;38:5081–5095.
14. Vardoulakis I, Papanastasiou P. Bifurcation analysis of deep boreholes: I. Surface instabilities. *Int J Numer Anal Methods Geomech*. 1988;12:379–399.
15. Papanastasiou P, Vardoulakis I. Bifurcation analysis of deep boreholes: II. Scale effect. *Int J Numer Anal Methods Geomech*. 1989;13:183–198.
16. Papamichos E, Vardoulakis I, Sulem J. Generalized continuum models for borehole stability analysis. In: *Proc. EUROCK '94 Rock Mechanics in Petroleum Engineering, Delft*. SPE/ISRM 28025, Balkema: Rotterdam; 1994, p. 37–44.
17. Sulem J, Vardoulakis I, Papamichos E. Microstructure and scale effect in granular rocks. In: Mühlhaus H-B, ed. *Continuum Models for Materials with Micro-Structure*. John Wiley & Sons; 1995, Chapter 7.
18. Papamichos E, van den Hoek PJ. Size dependency of castlegate and berea sandstone hollow-cylinder strength on the basis of bifurcation theory. In: Daemen JJK, Schultz RA, eds. *35th, U.S. Symp. on Rock Mechanics*. Balkema, Rotterdam: Lake Tahoe, CA; 1995, p. 301–306.
19. Papanastasiou P. Localization of deformation and failure around elliptical perforations based on a polar continuum. *Comput Mech*. 2000;26:352–361.
20. Papamichos E. Analysis of borehole failure modes and pore pressure effects. *Comput Geotech*. 2010;37:141–152. http://dx.doi.org/10.1016/j.compgeo.2009.08.006.
21. Papamichos E. Borehole failure analysis in a sandstone under anisotropic stresses. *Intl J Numer Anal Methods Geomech*. 2010;34:581–603. http://dx.doi.org/10.1002/nag.824.
22. Timoshenko SP, Goodier JN. *Theory of Elasticity*. McGraw-Hill; 1970.